JOURNAL OF GUIDANCE, CONTROL, AND DYNAMICS
Vol. 32, No. 5, September–October 2009

Spin-Axis Attitude Determination from Earth Chord-Angle Variations for Geostationary Satellites

Jozef C. van der Ha*
Kyushu University, Fukuoka 819-0395, Japan
and
Frank L. Janssens†
2201 KA Noordwijk, The Netherlands

DOI: 10.2514/1.40752

Spin stabilization offers a straightforward and robust concept for spacecraft attitude control. The spin-axis attitude determination is usually accomplished by means of sun- and Earth-sensor measurements. This paper explores techniques for spin-axis attitude determination using only Earth-sensor data. An immediate attitude determination can be achieved by straightforward geometrical arguments based on the extremes of the chord-angle variations over the orbit. Furthermore, an effective least-squares approach is presented that employs a number of equidistant chord-angle measurements collected during one orbital revolution. The adopted measurement model is favorable for reducing the adverse effects of systematic errors. Finally, a few explicit approaches are offered for reconstructing the most important biases. The application of these techniques is illustrated by means of actual telemetry data from the METEOSAT second-generation satellite MSG-2.

I. Introduction

SPIN-STABILIZATION offers a straightforward, cost-effective, and robust attitude stabilization concept for many mission applications. A combination of sun and Earth sensors is normally the most suitable means for performing the attitude determination (for spin rates in the range from about 5 to over 100 rpm). Usually, the measurements from both of these two sensors are employed in order to have two independent reference directions for the attitude determination algorithm.

There exists an extensive literature on the attitude determination of spinning spacecraft as exemplified by the standard reference, Wertz [1]. The spin-axis attitude determination is typically performed by least-squares estimation techniques [2,3] using batches of sensor measurement data. The accuracy of the resulting attitude solution is influenced by random errors as well as biases and unmodeled effects. The random-noise effects can be removed by using a sufficiently large set of data. The influences of the biases, however, cannot be eliminated completely in practice, and this represents the fundamental limit for the achievable attitude determination accuracy [4,5].

This paper presents a few straightforward but very effective approaches (which have not been presented in Wertz [1]) for spin-axis attitude determination using Earth-sensor data only. Applicable spacecraft have an Earth sensor with at least two infrared pencil beams at different mounting angles. When these pencil beams have simultaneous Earth coverage, the attitude knowledge can be established from the variations in the corresponding chord angles over the orbit. The main biases encountered in practice are errors in the Earth's infrared radiation profile, dynamical tilt and wobbling of the spin axis, and sensor misalignments. These biases represent the limiting factors for the attitude determination accuracy that can be achieved. The method presented here eliminates at least parts of these bias effects, namely those that act identically on the two chord angles measured by the two pencil beams. Furthermore, a few straightforward techniques are proposed for explicitly reconstructing these biases.

The nonlinear character of the attitude measurement equations presents many obstacles. The present paper offers attractive and straightforward techniques for avoiding these difficulties. A judicious choice of the measurement variable leads naturally to a least-squares formulation. This so-called "kappa-method" has proven its merits since 1978 in ESA's series of METEOSAT weather satellites in geostationary orbit. We also present a straightforward ad hoc method that produces an attitude solution from just the chord extrema for a satellite in a geostationary orbit. Finally, the geometric equal-chord method [4] is mentioned in the paper. This method may be employed in any orbit (as long as the two chords intersect) but requires additional information, like for instance a sun-aspect angle, to establish a complete attitude solution. The use of these methods has been illustrated by means of in-orbit sensor data from MSG-2 (METEOSAT second generation-2). The results show consistent attitude solutions even in the presence of significant unmodeled effects or biases.

II. Earth-Sensor Measurements

The Earth sensor has two static pencil beams oriented at angles $\mu_i (i = 1, 2)$ from the body-fixed spin axis (Z axis) as shown in Fig. 1 (for only one pencil beam). Strictly speaking, the dynamical spin-axis attitude is a unit vector along the angular momentum vector. We assume here that the angular momentum vector always coincides exactly with the body-fixed Z axis, which is an axis of either maximum or minimum inertia. Typical geostationary spinning satellites have their spin axis pointing in a direction close to the orbit normal (usually within 1 deg). When the pencil-beam pointing directions are within 5 deg from the spacecraft equator, both pencil beams can scan the favorable midlatitude regions of the Earth simultaneously. For instance, the European METEOSAT series of weather satellites use the values $\mu_1 \approx 86$ deg and $\mu_2 \approx 94$ deg.

The fundamental pencil-beam measurements are the space/Earth (S/E) and the Earth/space (E/S) pulses, which correspond to the

Presented at the 18th AAS/AIAA Space Flight Mechanics Meeting, Galveston, TX, 27–31 January 2008; received 2 September 2008; revision received 26 February 2009; accepted for publication 27 March 2009.

*Professor, Department of Aeronautics and Astronautics; jvdha@aol.com. Senior Member AIAA.
†Consultant; f.anssens@ziggo.nl.

crossing times of the Earth's infrared rim. These times can be converted into the half-chord angles $\kappa_i (i = 1, 2)$ for the two pencil beams by means of the spin rate. Knowledge of the spin rate can be established from the sun or Earth-sensor measurements. In this paper we assume that the spin rate remains constant over the interval considered.

The angle ρ in Fig. 1 is the *apparent Earth-radius angle* seen from geostationary altitude. From spherical geometry, we have (Wertz [1], equations 11-7, 8)

$$\cos\mu_i \cos\beta + \sin\mu_i \sin\beta \cos\kappa_i = \cos\rho \qquad (i = 1, 2) \qquad (1)$$

where the *Earth-aspect angle* (also known as nadir angle) β is the angle between the spin axis $\mathbf{Z}$ and the Earth vector $\mathbf{E}$, which is the spacecraft-to-Earth unit vector (see Fig. 1):

$$\beta(\nu) = \arccos\{\mathbf{Z} \cdot \mathbf{E}(\nu)\} \qquad (2)$$

The Earth vector $\mathbf{E}(\nu) = -\mathbf{r}(\nu)/r(\nu)$ varies with the orbital phase angle ν and points opposite to the orbital radius vector $\mathbf{r}(\nu)$.

Equation (1) can be used in different ways, for instance:

1) It allows to solve directly for β when the half-chord-angle measurements κ_i are inserted (but care must be taken to resolve the sign ambiguity);

2) It is useful as the measurement equation for a batch-type estimation of β.

For a general elliptical orbit, the apparent Earth-radius angle ρ varies with the satellite's orbital position $r(\nu)$ and the Earth's radius R_E:

$$\rho(\nu) = \arcsin\{R_E/r(\nu)\} \quad \text{with} \quad r(\nu) = \ell/\{1 + e\cos(\nu - \omega)\} \qquad (3)$$

The orbital elements ℓ, e, and ω denote the semilatus rectum, the eccentricity, and the argument of perigee, respectively. The orbital radius $r(\nu)$ is known from orbit determination. For a worst-case knowledge error Δr of 5 km, the error in ρ becomes $|\Delta\rho_r| = (\Delta r/r)\tan\rho < 0.001$ deg, which is negligible within the context of attitude determination.

The radius R_E in Eq. (3) is the Earth's *infrared* radius observed by the Earth sensor. The effective infrared radiation level at which the Earth sensor is designed to trigger is typically 50% of the observed peak radiance. The Earth's mean infrared radiance profile (in the CO_2 spectral band) reaches to about 40 km above the Earth's surface (Wertz [1], pp. 90–97). The uncertainty in the triggering altitude is hard to predict, but a value of 5 km is expected to be conservative. Because the mean radius of the solid Earth is about 6367.5 km, it follows that the mean infrared Earth radius $R_E \approx$ 6407.5 km and $\rho \approx 8.741$ deg at the geostationary orbital radius of 42,164 km. In practice, each of the two pencil beams may encounter different Earth radii because of a priori unknown temporal and local variations in the Earth's infrared profiles at the locations where the pencil beams have their S/E and E/S crossings (Fig. 1).

For geostationary satellites with pencil-beam settings within 5 deg from the spacecraft equator, the pencil-beam scan paths cross the Earth's rim in the midlatitude region. Obviously, the Earth oblateness affects the crossing times measurements with errors of the order of a few kilometers. The total Earth-sensor triggering error (including radiation profile and oblateness effects) remains well below 10 km and is negligible for geostationary satellites, that is, $|\Delta\rho| < 0.002$ deg.

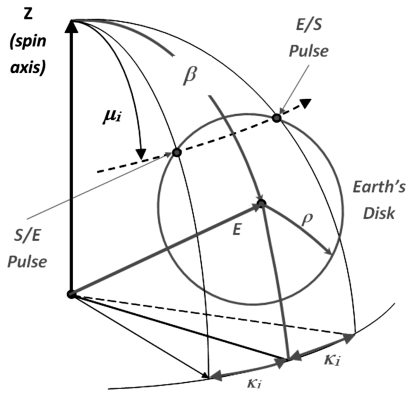

Fig. 1 Earth-sensor measurement principle.

To illustrate the evolution of the measurements, we solve for κ_i from Eq. (1):

$$\kappa_i(\nu) = \arccos\left\{\frac{\cos\rho(\nu) - \cos\mu_i\cos\beta(\nu)}{\sin\mu_i\sin\beta(\nu)}\right\} \qquad (i = 1, 2) \qquad (4)$$

Figure 2 shows the half-chord angles $\kappa_i (i = 1, 2)$ generated by the pencil-beams over a circular equatorial geostationary orbit. The pencil-beam settings are taken as $\mu_1 = 86$ deg and $\mu_2 = 94$ deg, and the spin-axis attitude used in the simulation has right ascension and declination angles of $\alpha = 0$ deg and $\delta = 89.9$ deg in inertial geocentric coordinates. Figure 2 shows that the two chords reach their alternating maximum and minimum values at the orbital phase angles $\nu \approx 0$ and 180 deg. At the orbital positions $\nu \approx 90$ and 270 deg, on the other hand, the two chords intersect. At these times, the so-called equal-chord condition (i.e., $\kappa_e = \kappa_1 = \kappa_2$) is satisfied.

III. Attitude and Orbit Interactions

We now address the geometrical relationships between the satellite orbit and the spin-axis attitude. This involves the representation of the attitude within the applicable reference frames (i.e., geocentric inertial, orbital, and nodal). We make use of the fact that the orbit is close to a perfect circular geostationary orbit with a small eccentricity e of at most 0.002 and a small inclination i of up to 1 deg.

A. Attitude in Inertial Frame

The spin-axis attitude is represented by the unit vector $\mathbf{Z}$. The inertial components of the attitude $\mathbf{Z}$ can be expressed in terms of its inertial right ascension α and declination δ, Fig. 3:

$$\mathbf{Z} = (\cos\alpha\cos\delta, \sin\alpha\cos\delta, \sin\delta)^T \qquad (5)$$

The orbital phase angle ν is defined with reference to the line of nodes. Therefore, the true anomaly (for an elliptical orbit) is ν-ω with ω the argument of perigee (not shown in Fig. 3). The general transformation matrix between the local orbit coordinates (x_{orb}, y_{orb}, z_{orb}) and the inertial coordinates (X_i, Y_i, Z_i) in Fig. 3 is given by

$$\begin{pmatrix} x_{\text{orb}} \\ y_{\text{orb}} \\ z_{\text{orb}} \end{pmatrix} = \begin{bmatrix} \cos\nu\cos\Omega - \sin\nu\cos i\sin\Omega & \cos\nu\sin\Omega + \sin\nu\cos i\cos\Omega & \sin\nu\sin i \\ -\sin\nu\cos\Omega - \cos\nu\cos i\sin\Omega & -\sin\nu\sin\Omega + \cos\nu\cos i\cos\Omega & \cos\nu\sin i \\ \sin i\sin\Omega & -\sin i\cos\Omega & \cos i \end{bmatrix} \begin{pmatrix} X_i \\ Y_i \\ Z_i \end{pmatrix} \qquad (6)$$

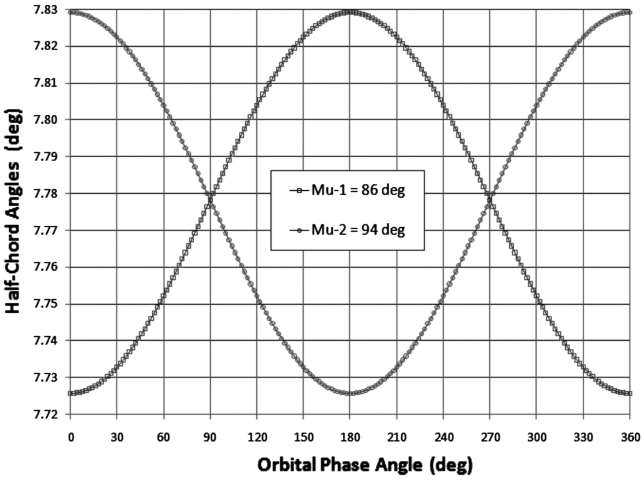

Fig. 2 Simulated half-chord angles for geostationary spacecraft ($\alpha = 0$; $\delta = 89.9$ deg).

The unit vector $\mathbf{n}_{\text{orb}}$ points normal to the orbit plane and is parallel to the z_{orb} axis of the satellite local orbital reference frame (Fig. 3) with inertial components:

$$\mathbf{n}_{\text{orb}} = (\sin i \sin\Omega, -\sin i \cos\Omega, \cos i)^T \tag{7}$$

The inner product of $\mathbf{Z}$ and $\mathbf{n}_{\text{orb}}$ is given by:

$$\mathbf{Z} \cdot \mathbf{n}_{\text{orb}} = \cos i \sin\delta - \sin i \cos\delta \sin(\alpha - \Omega) \tag{8}$$

The following special cases can be visualized with the help of Fig. 3:

$$\alpha = \Omega \pm 90\,\text{deg} \Rightarrow \mathbf{Z} \cdot \mathbf{n}_{\text{orb}} = \sin(\delta \mp i) \tag{9a}$$

$$\alpha = \Omega, \Omega + 180\,\text{deg} \Rightarrow \mathbf{Z} \cdot \mathbf{n}_{\text{orb}} = \cos i \sin\delta \tag{9b}$$

For small inclination angles we have $\mathbf{Z} \cdot \mathbf{n}_{\text{orb}} \approx \sin\delta$ regardless of the right ascension value α.

The condition for the attitude vector to be pointing normal to the orbit plane can be written as

$$\mathbf{Z} \cdot \mathbf{n}_{\text{orb}} = \cos i \sin\delta - \sin i \cos\delta \sin(\alpha - \Omega) = \pm 1 \tag{10}$$

This condition is satisfied when $i = 0$ and $\delta = \pm 90$ deg, which corresponds to the ideal geostationary situation. For a near-equatorial orbit with small inclination i and an attitude vector pointing close to the (north) normal of the Earth's equator with $\delta = 90\,\text{deg} - \varepsilon$ (with small positive ε), we find

$$\mathbf{Z} \cdot \mathbf{n}_{\text{orb}} \approx 1 - (i^2 + \varepsilon^2)/2 - i\varepsilon \sin(\alpha - \Omega) \tag{11}$$

with an error of third order in terms of the small parameters i and ε.

Therefore, the depointing angle φ between the attitude vector and the orbit normal is bounded by

$$\varphi = \arccos(\mathbf{Z} \cdot \mathbf{n}_{\text{orb}}) \leq i + \varepsilon \tag{12}$$

The Earth vector $\mathbf{E}$ points opposite to the x_{orb} axis, see Fig. 3. When neglecting second and higher terms in the small angles i and ε, we obtain the following result for $\mathbf{Z} \cdot \mathbf{E}(\nu)$:

$$\mathbf{Z} \cdot \mathbf{E}(\nu) \approx -\varepsilon \cos(\nu - \alpha + \Omega) - i \sin\nu \tag{13}$$

This confirms that the vectors $\mathbf{Z}$ and $\mathbf{E}$ point essentially normal to each other throughout the orbit.

B. Attitude in Orbit Frame

For the present geostationary application, it is most efficient to express the attitude vector in components within the orbit frame before executing the attitude determination procedure and to transform the attitude vector back to inertial components afterward. Therefore, we introduce the nodal reference frame (x_n, y_n, z_n) with its x_n and y_n axes within the orbit plane (Fig. 4). When the inclination is small, the transformation to the inertial frame may be approximated by

$$\begin{pmatrix} x_n \\ y_n \\ z_n \end{pmatrix} \approx \begin{bmatrix} \cos\Omega & \sin\Omega & 0 \\ -\sin\Omega & \cos\Omega & i \\ i\sin\Omega & -i\cos\Omega & 1 \end{bmatrix} \begin{pmatrix} X_i \\ Y_i \\ Z_i \end{pmatrix} \tag{14}$$

The components of the attitude vector relative to the nodal reference frame are written in the form of Eq. (5), but the angles α_o and δ_o are now defined in the (x_n, y_n, z_n) reference frame:

$$\mathbf{Z}_o = (\cos\alpha_o \cos\delta_o, \sin\alpha_o \cos\delta_o, \sin\delta_o)^T \tag{15}$$

It is straightforward to transform the components of $\mathbf{Z}_o$ back to its inertial representation $\mathbf{Z}$ by means of the inverse of the transformation matrix of Eq. (14):

$$\begin{pmatrix} \cos\alpha\cos\delta \\ \sin\alpha\cos\delta \\ \sin\delta \end{pmatrix} \approx \begin{bmatrix} \cos\Omega & -\sin\Omega & i\sin\Omega \\ \sin\Omega & \cos\Omega & -i\cos\Omega \\ 0 & i & 1 \end{bmatrix} \begin{pmatrix} \cos\alpha_o\cos\delta_o \\ \sin\alpha_o\cos\delta_o \\ \sin\delta_o \end{pmatrix} \tag{16}$$

Therefore

$$\tan\alpha \approx \tan(\alpha_o + \Omega) - i\frac{\tan\delta_o \cos\alpha_o}{\cos^2(\alpha_o + \Omega)} \tag{17a}$$

$$\sin\delta \approx \sin\delta_o + i \sin\alpha_o \cos\delta_o \tag{17b}$$

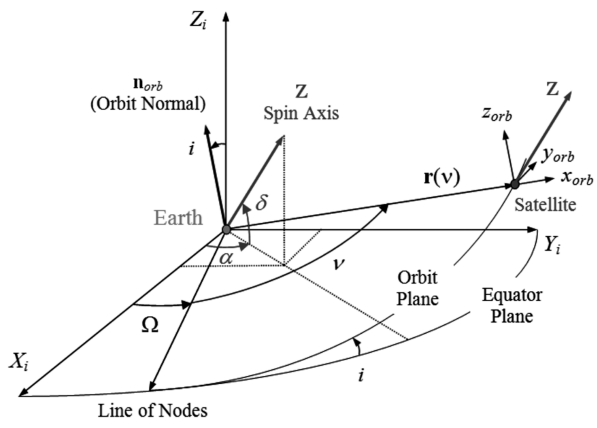

Fig. 3 Orbit and attitude geometry in inertial (X_i, Y_i, Z_i) frame.

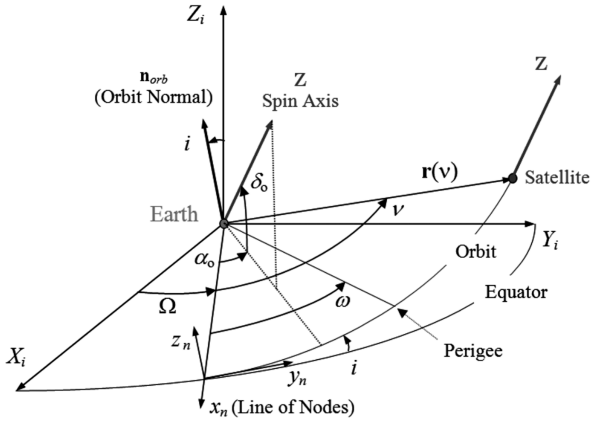

Fig. 4 Attitude geometry in orbital nodal (x_n, y_n, z_n) frame.

When $i = 0$, Eqs. (17a) and (17b) reduce to $\alpha = \alpha_o + \Omega$ and $\delta = \delta_o$, as expected.

The Earth-vector components within the (x_n, y_n, z_n) reference frame (Fig. 4) are given by

$$\mathbf{E}_o(\nu) = -\mathbf{r}(\nu)/r(\nu) = -(\cos\nu, \sin\nu, 0)^T \tag{18}$$

The inner product of $\mathbf{Z}_o$ and $\mathbf{E}_o(\nu)$ is thus

$$\mathbf{Z}_o \cdot \mathbf{E}_o(\nu) = -\cos(\nu - \alpha_o)\cos\delta_o \tag{19}$$

This result is a straightforward periodic function of the orbital phase angle ν and is more attractive than Eq. (13) because it is exact and the angles Ω and i are absent. Equation (19) indicates that the attitude points normal to the Earth vector in the following circumstances:

$$\mathbf{Z}_o \cdot \mathbf{E}_o(\nu) = 0 \Rightarrow \begin{cases} \delta_o = \pm\pi/2 \quad (\text{any } \nu) \text{ or:} \\ \nu_{1,2} = \alpha_o \pm \pi/2 \quad (\text{any } \delta_o) \end{cases} \tag{20}$$

In the first case, the attitude points normal to the orbit plane, whereas the second case refers to an arbitrary attitude orientation where the normality condition is fulfilled twice during each orbit.

The extremes of the Earth-aspect angle $\beta(\nu) = \arccos\{\mathbf{Z}_o \cdot \mathbf{E}_o(\nu)\}$ over the orbit are given by

$$\begin{aligned} &\mathbf{Z}_o \cdot \mathbf{E}_o(\nu) = -\cos\delta_o \Rightarrow \beta = \beta_{\max} = \pi - \delta_o, \quad \text{at } \nu_{\max} = \alpha_o \\ &\mathbf{Z}_o \cdot \mathbf{E}_o(\nu) = +\cos\delta_o \Rightarrow \beta = \beta_{\min} = \delta_o, \quad \text{at } \nu_{\min} = \alpha_o \pm \pi \end{aligned} \tag{21}$$

In the special case when $\delta_o = 90$ deg, the attitude vector $\mathbf{Z}_o$ points normal to the orbit plane and is thus normal to the Earth vector $\mathbf{E}_o(\nu)$ throughout the orbit, that is, $\beta(\nu) = 90$ deg for all ν. In fact, for most geostationary applications, the attitude declination angle δ_o remains very close to 90 deg. Therefore, the variations of $\beta(\nu)$ stay within narrow bounds around 90 deg (for instance, in Fig. 2, the maximum excursion is 0.1 deg).

C. Effect of Eccentricity

Most geostationary orbits have a small eccentricity of perhaps up to $e \approx 0.002$. This means that the apparent Earth-radius angle $\rho(\nu)$ exhibits small oscillations $\delta\rho(\nu) = \rho(\nu) - \rho_c$ over the orbit, and this affects the resulting chord measurements. From Eq. (3) we have

$$\sin\rho(\nu) = (R_E/\ell)(1 + p\cos\nu + q\sin\nu) \approx \sin\rho_c + \delta\rho(\nu)\cos\rho_c \tag{22}$$

The parameters $p = e\cos\omega$ and $q = e\sin\omega$ are the components of the eccentricity vector $\mathbf{e}$ along the nodal axes (x_n, y_n) of Fig. 4. The angle $\rho_c = \arcsin(R_E/r_c) \approx 8.741$ deg represents the apparent Earth infrared radius seen from geostationary altitude. The first-order approximation (in terms of small eccentricity) of $\delta\rho(\nu)$ follows from Eq. (22):

$$\delta\rho(\nu) \approx \tan\rho_c(p\cos\nu + q\sin\nu) \tag{23}$$

Equation (23) indicates that the amplitude of the periodic variations in the apparent Earth radius is $|\delta\rho| = e\tan\rho_c < 0.018$ deg for eccentricity values up to $e \approx 0.002$. The variation in the Earth radius over the orbit affects the half-chord-angle measurements in Eq. (1) through the term

$$\cos\rho(\nu) = \cos\{\rho_c + \delta\rho(\nu)\} \approx \cos\rho_c - \sin\rho_c\delta\rho(\nu) \tag{24}$$

The effect of $\delta\rho$ on the half-chord-angle measurement $\delta\kappa_i (i = 1, 2)$ can be established from the sensitivity relationship, which follows from Eqs. (1) and (24)

$$\delta\kappa_i = \frac{\partial\kappa_i}{\partial\rho}\delta\rho(\nu) = \sin\rho_c\delta\rho(\nu)/(\sin\kappa_i\sin\mu_i\sin\beta) \tag{25}$$

Because both μ_i and β are close to 90 deg (for geostationary applications) we can approximate $|\delta\kappa_i| \approx (\sin\rho_c/\sin\kappa_i)|\delta\rho|$ $< 1.13\,|\delta\rho| \approx 0.02$ deg. Because Earth-sensor calibration errors are typically a few hundredths of a degree, we conclude that the effect of orbit eccentricity on the chord measurements may be neglected (at least for values of e up to about 0.002).

IV. Geometric Attitude Determination

A. General Measurement Model

When subtracting the cosines of the half-chord-angle measurements κ_1 and κ_2 generated by the two pencil beams with mounting angles μ_1 and μ_2, respectively, we find from Eq. (4):

$$\begin{aligned} y = \cos\kappa_1 - \cos\kappa_2 &= \frac{2\sin d(\cos\mu\cos\rho - \cos d\cos\beta)}{(\cos^2 d - \cos^2\mu)\sin\beta} \\ &= \frac{b\cos\rho - a\cos\beta}{\sin\beta} \end{aligned} \tag{26}$$

Whereas the angles $\kappa_i (i = 1, 2)$, β, and ρ are functions of the orbital phase angle ν (as discussed in the preceding sections), the parameters μ, d, a, and b are constants defined as

$$\mu = (\mu_2 + \mu_1)/2 \tag{27a}$$

$$d = (\mu_2 - \mu_1)/2 \tag{27b}$$

$$a = \sin(2d)/(\cos^2 d - \cos^2\mu) \tag{27c}$$

$$b = 2\sin d\cos\mu/(\cos^2 d - \cos^2\mu) \tag{27d}$$

The (virtual) Earth-sensor angles μ and d stand for the mean value and half the difference, respectively, of the actual mounting angles μ_i with $i = 1, 2$ (Fig. 1).

An explicit expression for the unknown Earth-aspect angle $\beta(\nu)$ in terms of the differences of the cosines of the half-chord angles can be established by inversion of Eq. (26):

$$\beta_{1,2} = \arccos\left\{\left(aB \pm y\sqrt{(y^2 + a^2 - B^2}\right)/(y^2 + a^2)\right\} \tag{28}$$

with abbreviations $y = \cos\kappa_1 - \cos\kappa_2$ and $B = b\cos\rho$. Equation (28) is valid for two Earth-sensor pencil-beam measurements in any Earth orbit. Care must be taken that the proper sign is selected, for instance by using a priori knowledge of the evolution of the Earth-aspect angle β.

B. Specific Geostationary Application

Geostationary satellites usually have pencil-beam mounting angles that are symmetric relative to the spacecraft equator, and so their nominal mean value $\mu = 90$ deg. In this case, the constant parameter a in Eq. (27c) becomes $a = 2\tan d$ and the parameter b in Eq. (27d) vanishes. For the sake of generality, and in order to accommodate sensor misalignments and other biases, the term containing b in Eq. (26) will be carried along in the subsequent analysis.

Most geostationary satellites have their spin axis directed close to the Z_i axis of the inertial frame, which points normal to the Earth equator. As long as the orbit inclination remains small, the spin axis will be close to the orbit normal and the Earth-aspect angle $\beta \approx 90$ deg throughout the orbit. Therefore, it is useful to introduce the small angle $\delta\beta = \beta - \pi/2$. Furthermore, the eccentricity effect will be neglected so that $\rho(\nu) \approx \rho_c$. Equation (26) can now be expressed as

$$y = \cos\kappa_1 - \cos\kappa_2 = (b\cos\rho_c + a\sin\delta\beta)/\cos\delta\beta \tag{29}$$

It is of interest to employ the series expansion of the main term $\tan\delta\beta$ for small values of $\delta\beta$:

$$\tan(\delta\beta) \approx \delta\beta + \frac{1}{3}(\delta\beta)^3 + \frac{2}{15}(\delta\beta)^5 + O\{(\delta\beta)^7\} \tag{30}$$

The $(\delta\beta)^5$ term is below 1 arcs for $\delta\beta$ angles up to 7.4 deg and is obviously negligible. The $(\delta\beta)^3$ term is less than 0.001 deg for $\delta\beta$ angles up to 2.1 deg and can also be neglected for practically all applications. The magnitude of b is typically of the same order as $(\delta\beta)^2$. When neglecting terms of the order of $(\delta\beta)^3$, we can express Eq. (29) as

$$y = \cos\kappa_1 - \cos\kappa_2 \approx b\cos\rho_c + a\delta\beta \tag{31}$$

This measurement equation shows a *linear* relationship between the measurement y and the attitude represented by the angle $\delta\beta$. The parameters a and b depend only on the sensor mounting angles and can be kept constant during the attitude estimation process. The mean value of the measurements is the constant term $b\cos\rho$, which vanishes when $\mu = 90$ deg, see Eq. (27d).

C. Geometry of Chord Measurements

At specific points in the orbit it is possible to determine the Earth-aspect angle (and sometimes the spin-axis attitude as well) from purely geometrical considerations. Figure 5 shows the spin-axis direction, which is pointing slightly away from the orbit normal by the small angle ε. At the orbital positions 1 and 2, the spin-axis attitude points perpendicular to the instantaneous Earth vector. Therefore, the Earth-aspect angle β equals 90 deg at these positions.

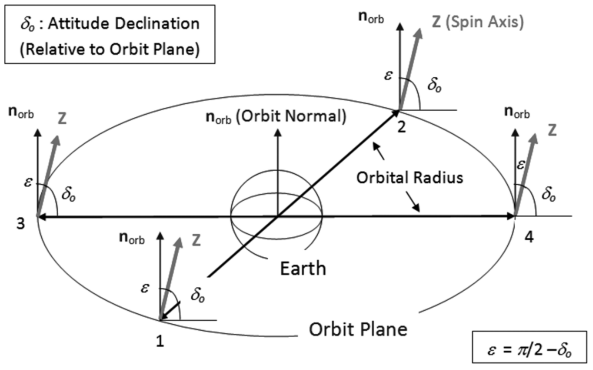

Fig. 5 Attitude-orbit geometry at four orbital positions.

At the positions 3 and 4, on the other hand, the spin axis lies within the plane defined by the instantaneous Earth vector and the orbit-normal vector $\mathbf{n}_{\text{orb}}$. It is evident that the Earth-aspect angle β reaches its extreme excursions away from 90 deg at these two points.

The corresponding pencil-beam scan paths over the Earth are sketched in Figs. 6a–6d. They show the two pencil-beam scans as seen from the spacecraft for each of the four selected orbital positions 1, 2, 3, and 4 in Fig. 5. Under ideal conditions, namely a circular geostationary orbit, a perfectly spherical Earth, a constant spin-axis attitude orientation pointing normal to the orbit plane, and pencil beams that are mounted symmetrically to the spacecraft equator, all scans shown in Figs. 6a–6d would have identical lengths. If the attitude is not normal to the orbit, however, the centerline of the two pencil-beam scans makes an angle $\varepsilon = \pi/2 - \delta_o$ with the projection of the orbit plane on the Earth as shown in Figs. 6a–6d, see also Eqs. (18–21).

It can be seen that the measured chord angles at positions 1 and 2 of Fig. 5 (corresponding to the Figs. 6a and 6b) are identical even when $\varepsilon \neq 0$ so that the equal-chord condition is satisfied here. At positions 3 and 4 of Fig. 5 (and also Figs. 6c and 6d), the scans are displaced downward and upward relative to the centerline by an extreme amount. These cases represent the minimum and maximum measured chord angles over the orbit. In an ideal circular orbit, the four positions shown in Fig. 5 would be separated by exactly 90 deg (i.e., a quarter orbital period). For small eccentricity values (up to $e = 0.002$) the lengths of these intervals may vary by at most 0.5 min or 0.12 deg.

D. Equal-Chord Condition

The equal-chord method [4] uses half-chord-angle measurements collected at the times when the chords produced by the two pencil beams are identical as happens at positions 1 and 2 in Figs. 5, 6a, and 6b. The method produces an immediate geometrical solution for the Earth-aspect angle $\beta_e = \beta(t_e)$ at the equal-chord time t_e.

When considering the case $\mu \approx 90$ deg, which implies that $b \approx 0$, see Eq. (27d), we find from Eq. (26) that $\cot(\beta_e)$ must vanish at the time t_e. Therefore, the Earth-aspect angle $\beta_e = \beta(t_e)$ must be equal to 90 deg and Eq. (1) produces the results

$$\sin\mu_1\cos\kappa_e = \sin\mu_2\cos\kappa_e = \cos\rho_c \tag{32a}$$

$$\Rightarrow \kappa_e = \arccos\{\cos\rho_c/\cos d\} \tag{32b}$$

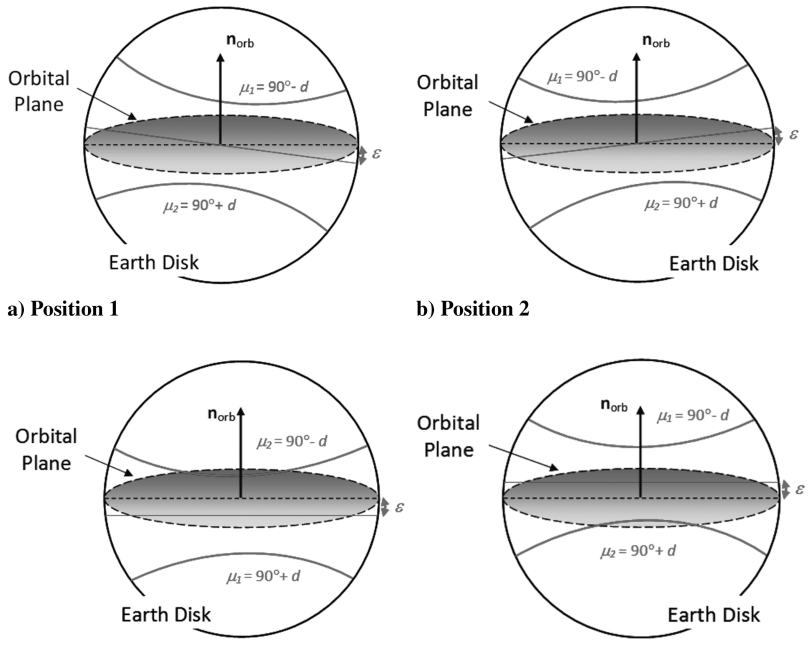

Fig. 6 Pencil-beam scan paths for the four positions of Fig. 5.

This equal-chord solution is mathematically meaningful only if the condition $d \leq \rho_c$ is satisfied. When this condition is violated, the pencil beams are too wide apart to be able to cross the Earth's disk simultaneously and there simply cannot be an equal-chord occurrence.

For a perfectly circular geostationary orbit, the apparent Earth angle remains constant, that is, $\rho_c \approx 8.741$ deg as calculated following Eq. (22). Therefore, the equal-chord angle κ_e can be predicted a priori (i.e., before any measurements have been collected) based on the knowledge of the apparent Earth-radius angle and the sensor mounting angles. For instance, in the case when $\mu = 90$ deg and $d = 4$ deg, Eq. (32b) immediately produces $\kappa_e \approx 7.778$ deg, which is consistent with the simulation results in Fig. 2. If the measured equal-chord angle $\kappa_e = \kappa(t_e)$ would deviate from the expected value, the residual would be useful for reconstructing the bias in ρ_c.

The equal-chord condition corresponds to the two orbital positions $\nu_e = \nu(t_e)$, that is, positions 1 and 2 in Fig. 5, where the attitude vector is oriented precisely normal to the instantaneous Earth vector. This implies that the right ascension α_o of the attitude vector is 90 deg ahead or behind the orbital position ν_e at the time t_e as can be seen from the second line in Eq. (20) and Fig. 5. Thus, the equal-chord positions allow the determination of the attitude right ascension angle α_o. The attitude declination angle δ_o, however, cannot be determined from the equal-chord condition by itself. Additional information, for instance the sun-aspect angle $\theta_e = \theta(t_e)$, is required to be able to establish a full attitude determination based on equal-chord measurements alone.

E. Attitude from Chord Extremes

Figures 5 and 6 indicate that the extremes of the chord angles are reached at the orbital positions 3 and 4. In fact, the Earth-aspect angle $\beta(\nu)$ also reaches its extreme value at these locations. Furthermore, the attitude right ascension and declination angles α_o and δ_o are related to the extremes of the Earth-aspect angle as shown by Eq. (21):

$$\delta_o = \pi - \beta_{\max}, \quad \text{at } \nu_{\max} = \alpha_o \tag{33a}$$

$$\delta_o = \beta_{\min}, \quad \text{at } \nu_{\min} = \alpha_o \pm \pi \tag{33b}$$

These results form the basis for a straightforward attitude determination procedure that produces *complete* attitude knowledge without requiring any further information.

The Earth-aspect angles $\beta_{\max}$ and $\beta_{\min}$ can be calculated from $y_{\max}$ and $y_{\min}$ using the two half-chord-angle measurements κ_1 and κ_2 at the positions $\nu_{\max}$ and $\nu_{\min}$, see Eq. (31):

$$\beta_{\max} = \pi/2 + \delta\beta_{\max} = \pi/2 + y_{\max} - b\cos\rho_c/a, \quad \text{at } \nu_{\max} = \alpha_o \tag{34a}$$

$$\beta_{\min} = \pi/2 + \delta\beta_{\min} = \pi/2 + y_{\min} - b\cos\rho_c/a \quad \text{at } \nu_{\min} = \alpha_o \pm \pi \tag{34b}$$

We note that Eqs. (33a) and (33b) indicate that the sum of $\beta_{\max}$ and $\beta_{\min}$ equals 180 deg, and, furthermore, $\delta\beta_{\max} = -\delta\beta_{\min}$. By adding the two Eqs. (34a) and (34b) we obtain an interesting result that allows the reconstruction of the parameter β from the extremes of the chord measurements:

$$b = (y_{\max} + y_{\min})/(2\cos\rho_c) \tag{35}$$

The average of the left- and right-hand sides of the two Eqs. (33a) and (33b) produces an accurate determination of the angle δ_o because the term $b\cos\rho_c$ (including its biases) will be eliminated:

$$\delta_o = \pi/2 - (\beta_{\max} - \beta_{\min})/2 = \pi/2 - (y_{\max} - y_{\min})/(2a) \tag{36}$$

where the expressions in Eqs. (34a) and (34b) have been used.

The angles $\nu_{\max} = \alpha_o$ and $\nu_{\min} = \alpha_o \pm \pi$ in Eqs. (33a) and (33b) correspond to the positions 3 and 4 in Figs. 5 and 6, respectively. The attitude angle α_o can immediately be determined as the average of these two orbital positions, that is the average of $\nu_{\max}$ and $\nu_{\min} \pm 90$ deg. The averaging is beneficial for reducing any biases contributed, for instance, by eccentricity effects. However, it should be noted that the right ascension angles constructed from the equal-chord positions are in general more accurate as can be understood from geometrical arguments (see Fig. 1 and 2).

Finally, the desired inertial attitude solution in terms of the angles (α, δ) can be obtained from the attitude angles α_o and δ_o by means of the transformation in Eqs. (16) and (17).

V. Batch Least-Squares Attitude Estimate

A. Measurement Equation

Equation (31) can be interpreted as the *measurement equation* describing the functional relationship between the measurements $y_j (j = 1, 2, \ldots, n)$ and the unknown state parameter $\delta\beta$. A batch of measurements spread out over a full orbit revolution can be used to determine the attitude associated with that orbit. An attitude estimation procedure will now be formulated on the basis of an optimal least-squares curve-fitting technique by using Eq. (31):

$$y_j = \cos\kappa_1(\nu_j) - \cos\kappa_2(\nu_j) = a\delta\beta(\nu_j) + b\cos\rho_c + w_j \quad (j = 1, 2, \ldots, n) \tag{37}$$

where $w_j (j = 1, 2, \ldots, n)$ represents the random-noise contributions (with mean value assumed to be zero).

We recall the geometrical relationship between the Earth-aspect angle $\beta(\nu_j)$ and the spin-axis attitude in terms of the angles α_o and δ_o (relative to the nodal frame) in Eq. (19):

$$\delta\beta(\nu_j) = \beta(\nu_j) - \pi/2 = \arcsin\{\cos(\nu_j - \alpha_o)\cos\delta_o\} \tag{38}$$

It is justified to linearize the arcsin term in Eq. (38) when δ_o is near 90 deg and $\delta\beta(\nu_j)$ is small (with error less than 0.001 deg for $\delta\beta < 2.7$ deg). The first term on the right-hand side of Eq. (37) is

$$a\delta\beta(\nu_j) \approx a\cos(\nu_j - \alpha_o)\cos\delta_o = c_1\sin\nu_j + c_2\cos\nu_j \tag{39}$$

The coefficients $c_k (\kappa = 1, 2)$ are related to the attitude vector components as follows:

$$c_1 = a\sin\alpha_o\cos\delta_o; \qquad c_2 = a\cos\alpha_o\cos\delta_o \tag{40}$$

After the coefficients $c_k (k = 1, 2)$ have been determined, the attitude angles (relative to the orbital plane) follow from

$$\alpha_o = \arctan\{c_1/c_2\}; \qquad \delta_o = \arccos\{\sqrt{(c_1^2 + c_2^2)}/a\} \tag{41}$$

This result may then be transformed into the inertial representation of the attitude by using Eqs. (16) and (17).

B. Least-Squares Model

The least-squares fitting procedure [6] uses a linear relationship between the observations and a set of independent basic functions with constant coefficients that are expected to generate these observations. Equations (37) and (39) suggest the following set of functions:

$$h_0(\nu) = 1; \qquad h_1(\nu) = \sin\nu; \qquad h_2(\nu) = \cos\nu \tag{42}$$

Equation (37) can be expressed in these functions as follows:

$$y_j = y(\nu_j) = \sum_{k=0}^{2} c_k h_k(\nu_j) + w_j \Rightarrow \mathbf{y} = H\mathbf{c} + \mathbf{w} \tag{43}$$

The measurement and random-noise vectors are n dimensional, that is, $\mathbf{y} = (y_1, y_2 \ldots, y_n)^T$ and $\mathbf{w} = (w_1, w_2 \ldots, w_n)^T$, respectively. The state vector that must be estimated consists of the three

coefficients $\mathbf{c} = (c_0, c_1, c_2)^T$ with c_1 and c_2 representing the attitude as shown in Eqs. (40) and (41).

The constant term represented by the coefficient c_0 corresponds to the parameter $b \cos \rho_c$ of Eq. (37). Its estimate allows us to evaluate the consistency of our assumed knowledge of the sensor mounting angles (i.e., μ and d) and the Earth-radius angle ρ_c with the estimate from the actual measurements. In geostationary applications, the parameter b follows from the estimate of c_0 when using the assumed value of the Earth-radius angle ρ_c. A deviation of the parameter b from its expected value points to the presence of biases (details are given in later sections).

The $n \times 3$-dimensional measurement matrix H stands for

$$H = \begin{bmatrix} 1 & \sin \nu_1 & \cos \nu_1 \\ 1 & \sin \nu_2 & \cos \nu_2 \\ \cdots & \cdots & \cdots \\ 1 & \sin \nu_n & \cos \nu_n \end{bmatrix} \tag{44}$$

The optimal least-squares estimate of the vector $\mathbf{c}$ equals the pseudoinverse solution, see, for instance, equation (1.26) of [6]:

$$\hat{\mathbf{c}} = (H^T H)^{-1} H^T \mathbf{y} \tag{45}$$

All measurements have the same weights because there is no obvious a priori criterion for assigning different weights to the individual measurements in the present application.

It is of interest to note that the matrix $(H^T H)$ and its inverse can be calculated explicitly for a set of measurements that are sampled at equal distances over the interval (0, 360 deg):

$$(H^T H) = \sum_{j=1}^{n} \begin{bmatrix} 1 & \sin \nu_j & \cos \nu_j \\ \sin \nu_j & \sin^2 \nu_j & \sin \nu_j \cos \nu_j \\ \cos \nu_j & \sin \nu_j \cos \nu_j & \cos^2 \nu_j \end{bmatrix} = n \begin{bmatrix} 1 & 0 & 0 \\ 0 & 0.5 & 0 \\ 0 & 0 & 0.5 \end{bmatrix} \tag{46a}$$

$$\Rightarrow (H^T H)^{-1} = \frac{1}{n} \begin{bmatrix} 1 & 0 & 0 \\ 0 & 2 & 0 \\ 0 & 0 & 2 \end{bmatrix} \tag{46b}$$

The estimates of the coefficients $\mathbf{c}$ can thus be expressed explicitly in terms of the measurements

$$\hat{\mathbf{c}} = (H^T H)^{-1} H^T \mathbf{y} = \frac{1}{n} \sum_{j=1}^{n} \begin{pmatrix} y_j \\ 2 y_j \sin \nu_j \\ 2 y_j \cos \nu_j \end{pmatrix} \tag{47}$$

For instance, if we collect four equidistant (i.e., separated by 90 deg) measurement samples $y_j (j = 1, \ldots, 4)$ over an orbital revolution, we obtain the plausible result

$$\hat{\mathbf{c}} = \begin{pmatrix} \hat{c}_0 \\ \hat{c}_1 \\ \hat{c}_2 \end{pmatrix} = \frac{1}{4} \begin{pmatrix} (y_1 + y_2 + y_3 + y_4) \\ 2(y_2 - y_4) \\ 2(y_1 - y_3) \end{pmatrix} \tag{48}$$

In general, the error covariance matrix of the estimate $\hat{\mathbf{c}}$ can readily be calculated from Eq. (45) using the explicit result for $(H^T H)^{-1}$ in Eq. (46b). It can be shown that the errors of the components in Eq. (48) are uncorrelated and we have

$$\sigma_0^2 = E\{(\Delta c_0)^2\} = \sigma_y^2 / n; \qquad \sigma_j^2 = E\{(\Delta c_j)^2\} = 2\sigma_y^2 / n \quad (j = 1, 2) \tag{49}$$

As expected, the estimation error decreases with the inverse square root of the n measurements.

VI. Error Analyses

A. Half-Chord-Angle Error

The fundamental pencil-beam measurements consist of the S/E and E/S crossing times of the Earth's infrared horizon (Fig. 1). These times can be transformed to the half-chord angles κ_i for each of the two pencil-beams:

$$\kappa_i = \omega_{\text{spin}} (t_{i,E/S} - t_{i,S/E})/2 \qquad (i = 1, 2) \tag{50}$$

where ω_{spin} denotes the spin rate, which is assumed to be constant and perfectly known. In an estimation process, the two crossing times in Eq. (50) may be treated as independent random variables. It is customary to assume that the random measurement errors in the crossing times are distributed in accordance with a Gaussian probability density function (PDF). In the absence of biases, the expected values of the measurements will correspond to the true crossing times. We assume that the standard deviations of all crossing times have the same value σ_t. It can be seen that the induced random variable κ (the index i is dropped now for convenience) in Eq. (50) is also Gaussian with expected value $\bar{\kappa} = \omega_{\text{spin}} (\bar{t}_{E/S} - \bar{t}_{S/E})$ and standard deviation $\sigma_\kappa = 1/2\sqrt{2}\omega_{\text{spin}}\sigma_t$.

The PDF of the random variable $x = \cos \kappa$ can be obtained through a transformation from the PDF of the Gaussian variable κ but the PDF of x is definitely not a Gaussian distribution. We separate κ in its true value κ_{true} plus a Gaussian variable $\Delta\kappa$ with zero expectation. The measurement κ satisfies $\cos \kappa = \cos \kappa_{\text{true}} - \sin \kappa_{\text{true}} \Delta\kappa$ with $\Delta\kappa \ll \kappa_{\text{true}}$ for scan paths far away from the Earth's limb. This approach can be used to establish the statistical properties of the random-noise term $\mathbf{w}$ on the right-hand side of our measurement Eq. (43).

Finally, we note that the model presented here also serves to include small nutation effects because they affect the measured chord angles in much the same way as the random noise.

B. Error in Observation *y*

We consider the propagation of arbitrary errors $\Delta\kappa_i, i = 1, 2$, with expected values $E\{\Delta\kappa_i\} = 0$, into the observation vector y defined in Eq. (37). The error Δy follows from the half-chord-angle errors $\Delta\kappa_i (i = 1, 2)$:

$$\Delta y = (-\sin \kappa_1, \sin \kappa_2) \begin{pmatrix} \Delta\kappa_1 \\ \Delta\kappa_2 \end{pmatrix} \tag{51}$$

The covariance of y can be calculated as

$$\sigma_y^2 = E\{(\Delta y)^2\} = (-\sin \kappa_1, \sin \kappa_2) \begin{pmatrix} E\{(\Delta\kappa_1)^2\} & E\{\Delta\kappa_1 \Delta\kappa_2\} \\ E\{\Delta\kappa_1 \Delta\kappa_2\} & E\{(\Delta\kappa_2)^2\} \end{pmatrix} \begin{pmatrix} -\sin \kappa_1 \\ \sin \kappa_2 \end{pmatrix} \tag{52}$$

We make a few reasonable assumptions about the nature of the chord-angle errors, namely that the measurement errors of each of the pencil beams have the same covariances $\sigma_\kappa^2 = E\{(\Delta\kappa_1)^2\} = E\{(\Delta\kappa_2)^2\}$ and are independent, $E\{\Delta\kappa_1 \Delta\kappa_2\} = 0$. Equation (52) can now be simplified as

$$\sigma_y^2 = \sigma_\kappa^2 (\sin^2 \kappa_1 + \sin^2 \kappa_2) \approx 2\sigma_\kappa^2 \sin^2 \tilde{\kappa} \tag{53}$$

where $\tilde{\kappa}$ is a representative value for both κ_i, $i = 1, 2$. This approximation is justified because the variations in the two chords are typically only a fraction of a degree. When taking $\tilde{\kappa} \approx 7.78$ deg (see Fig. 2), we find the approximate result

$$\sigma_y \approx \sqrt{2}\sigma_\kappa \sin \tilde{\kappa} \approx 0.191\sigma_\kappa \tag{54}$$

It is of interest to note that the expected error in the variable y is considerably smaller than the chord measurement errors themselves.

C. Attitude Error

The expected error in the attitude estimate can be established by recognizing that the coefficients c_1 and c_2 are proportional to the components of the spin-axis attitude vector along the nodal axes in the orbit plane. The comparison of Eqs. (15) and (40) shows immediately that $c_1 = aZ_{o,y}$ and $c_2 = aZ_{o,x}$. The variance of the projected component of the attitude vector within the orbit plane can be calculated from the results in Eq. (49):

$$|\Delta\mathbf{Z}_o| = \sqrt{(\Delta Z_{o,x})^2 + (\Delta Z_{o,y})^2} = \sqrt{\{(\Delta c_1)^2 + (\Delta c_2)^2\}}/a$$

$$\Rightarrow \sigma_{\text{att}} = \sqrt{\{\sigma_1^2 + \sigma_2^2\}}/a = 2\sigma_y/(a\sqrt{n}) \tag{55}$$

The nominal sensor values assumed here lead to $a \approx 0.140$. With the help of Eq. (54), we can express the attitude error in the half-chord error σ_κ:

$$\sigma_{\text{att}} \approx 2.72\,\sigma_\kappa/\sqrt{n} \tag{56}$$

Typical random errors in the half-chord-angle measurements may be of the order of $\sigma_\kappa \approx 0.025$ deg. When taking a set of 90 equidistant measurements per orbit, we find the expected attitude error when only random-noise effects are considered:

$$\sigma_{\text{att}} \approx 2.73\,\sigma_\kappa/\sqrt{90} \approx 0.007 \text{ deg} \tag{57}$$

This result confirms that the effect of the random errors will be reduced to insignificance when using a batch of 90 measurements collected at a 4 deg sampling interval over one orbit.

VII. Reconstruction of Biases

A. Sensor Pointing Biases

The sensor angles μ_i are measured accurately relative to the satellite's geometric Z axis before launch. After launch, the moments of inertia and the dynamical spin axis usually vary over time mainly because of the depletion of the onboard propellant. The tilt in the dynamical spin axis relative to the body Z axis directly affects the effective sensor orientation angle μ. Errors in the separation angle d between the two pencil beams, on the other hand, are due to relatively minor sensor-internal misalignments. Usually, the bias in d is insignificant when compared with biases in the angle μ and in the Earth's infrared horizon.

Small individual biases $\Delta\mu$ and Δd with respect to their nominal design values (for instance, $\mu = 90$ deg and $d = 4$ deg, respectively) affect the observation $y = \cos\kappa_1 - \cos\kappa_2$ through the auxiliary mounting parameters a and b defined in Eqs. (27c) and (27d). The sensitivity relationship can be established from Eq. (31):

$$\Delta y = (\delta\beta)\Delta a + (\cos\rho_c)\Delta b \tag{58}$$

The errors Δa and Δb follow from the biases $\Delta\mu$ and Δd:

$$\Delta a = (\partial a/\partial\mu)\Delta\mu + (\partial a/\partial d)\Delta d \tag{59a}$$

$$\Delta b = (\partial b/\partial\mu)\Delta\mu + (\partial b/\partial d)\Delta d \tag{59b}$$

When assuming $\mu \approx 90$ deg and $d \approx 4$ deg we can calculate the partial derivatives:

$$\partial a/\partial\mu \approx 2\sin d\sin(2\mu)/(\cos^3 d) \approx 0 \tag{60a}$$

$$\partial b/\partial\mu = -2\sin d\sin\mu/(\cos^2 d) \approx -2d \tag{60b}$$

$$\partial a/\partial d \approx 2/(\cos^2 d) \approx 2 \tag{60c}$$

$$\partial b/\partial d \approx 2\cos\mu(1 + \sin^2 d)/(\cos^3 d) \approx 0 \tag{60d}$$

Finally, the sensitivity of y with respect to sensor biases follows from Eq. (58):

$$\Delta y \approx 2(\delta\beta)\Delta d - 2(d\cos\rho_c)\Delta\mu \tag{61}$$

In practice, Δy can be interpreted as the "measurement residual," which is defined as the mean value (over some orbital arc) of the differences between the estimated observations $\tilde{y}_j$ (which can be generated from the available attitude estimate) and the actual measurements y_j, $j = 1, 2, \ldots, n$.

At the beginning of this section it was mentioned that the bias $\Delta\mu$ is typically more significant than the bias Δd. Furthermore, the coefficient of $\Delta\mu$, that is, the term $d\cos\rho_c$, in Eq. (61) is larger than the coefficient $\delta\beta$ of Δd. Therefore, Eq. (61) provides a straightforward and useful procedure for reconstructing the bias $\Delta\mu$ from the observed residual Δy:

$$\Delta\mu \approx -\Delta y/(2d\cos\rho_c) \approx -7.25\Delta y \tag{62}$$

This result illustrates that the sensitivity for reconstructing the bias $\Delta\mu$ from the observed residual Δy is extremely favorable.

B. Earth-Radius Bias

Equations (1) and (4) indicate that a bias in the Earth's infrared radius affects the chord measurements. The expected value of the infrared Earth radius is approximately 40 km above the Earth's solid disk (Wertz [1] p. 97). However, in practice, there are appreciable local (as well as temporal) variations about the nominal infrared radius. In particular, there is a north–south gradient due to seasonal influences, which can lead to significant errors in the measured half-chord angles of up to 0.3 deg [7].

In the case when the errors in the infrared radius are approximately uniform over the Earth's disk, the present model in terms of $y = \cos\kappa_1 - \cos\kappa_2$ is very attractive. Equation (31) shows that the variation of y under a constant change in Earth radius is given by $\Delta y \approx -(b\sin\rho_c)\Delta\rho$. Because $\mu \approx 90$ deg for geostationary applications, we find $b \approx 0$ and $\Delta y \approx 0$. Thus, the uniform biases in the Earth radii essentially vanish in the calculation of y. However, the nonuniform parts of the Earth's infrared radiation do not cancel and represent a significant error source for the attitude determination [7].

The equal-chord angle is useful for reconstructing the uniform bias in the apparent Earth-radius angle. Although the infrared biases vary locally, the equal-chord conditions occur at favorable midlatitude locations (see Figs. 6a and 6b) and may be representative for the uniform bias. The predicted half-chord-angle measurement at the equal-chord time is given by Eq. (32b):

$$\kappa_{e,\text{pred}} = \arccos\{\cos\rho_c/\cos d\} \tag{63}$$

The residual $\Delta\kappa_e$ between the measured equal-chord angle κ_e and its predicted value $\kappa_{e,\text{pred}}$ is most likely caused by an offset in the apparent Earth-radius angle ρ_c at the equal-chord time t_e. From Eq. (63) we find

$$\Delta\rho_e = \{\cos d\sin\kappa_e/\sin\rho_c\}\Delta\kappa_e \approx 0.888\Delta\kappa_e \tag{64}$$

This result gives a straightforward but useful approach for reconstructing the Earth-radius bias from the observed residual of the measured equal-chord angle κ_e at time t_e. It may be noted that a residual of 0.05 deg in the half-chord angle would correspond to an offset of about 32 km in Earth radius in the present application.

VIII. Application to MSG-2 Data

The techniques proposed previously have been illustrated by using actual in-orbit Earth-sensor data produced by MSG-2, which is the second operational flight in the series of METEOSAT second generation weather satellites.

Table 1 Summary of least-squares results and consequences

Number of data points	Attitude difference, deg	c_0, average value of $y(\nu)$	b, mounting parameter	$\Delta\mu$, mounting bias, deg
5	0.333	-4.36×10^{-4}	-4.41×10^{-4}	0.231
10	0.295	-4.29×10^{-4}	-4.35×10^{-4}	0.229
20	0.237	-3.76×10^{-4}	-3.80×10^{-4}	0.206
30	0.241	-3.04×10^{-4}	-3.08×10^{-4}	0.177
60	0.185	-3.31×10^{-4}	-3.35×10^{-4}	0.188
100	0.086	-3.60×10^{-4}	-3.64×10^{-4}	0.200
200	0.119	-3.57×10^{-4}	-3.61×10^{-4}	0.199
400	0.104	-3.54×10^{-4}	-3.58×10^{-4}	0.198
600	0.204	-3.61×10^{-4}	-3.65×10^{-4}	0.200
800	0.097	-3.52×10^{-4}	-3.57×10^{-4}	0.197
1000	0.256	-3.65×10^{-4}	-3.70×10^{-4}	0.202

A. Background

MSG-2 was injected into a geostationary transfer orbit by an Ariane 5 launcher on 21 December 2005. The initial operations [8] were conducted by ESA/European Space Operations Centre (ESOC) in Darmstadt, Germany and lasted until 2 January 2006, when MSG-2 achieved its geostationary operational phase and was handed over to the European Organisation for the Exploitation of Meteorological Satellites, known as EUMETSAT, also in Darmstadt, Germany.

The sensor data used in the present study cover a 24-h interval near the end of the near-geostationary drift phase, between 1800 h on 29 December and 1800 h on 30 December 2005. December 29 started out with an apogee-lowering maneuver and the releases of the baffle and cooler cover, followed by a collision avoidance maneuver [9]. Subsequently, the final spin up was performed in two parts, first to 90 rpm and finally to 99.782 rpm. Between about 900 and 1300 h, the propellant lines were decontaminated by heating. This lead to migration of propellant between the tanks and induced a persistent "wobbling motion," which affected the sensor data over the next few days. Finally, at 1400 h, the commissioning tests of the imager's scan mirror were performed.

At the start of the data interval, the spin-axis attitude was at an angle of about 3.5 deg from the orbit normal. This angle is considerably larger than during the operational geostationary phase. Therefore, the data offer adverse conditions for the methods presented in this paper, which are based on a close alignment between the attitude vector and the orbit-normal direction. The orbit eccentricity of 1.3×10^{-3} leads to altitude variations of about 55 km with corresponding variations in the apparent Earth-radius angle of about 0.012 deg. Furthermore, this eccentricity may cause measurements that are equidistant in time to be displaced by up to 0.08 deg in orbital position.

Throughout the interval considered here, the satellite attitude was in a free-drift mode without any control actuations. The dominant disturbing torque acting on the satellite is due to solar radiation pressure effects. Its cumulative effect over a one-day period can be considered negligible when considering a satellite spinning at about 100 rpm [10]. Therefore, the angular momentum vector may be taken constant.

B. Results of Least-Squares Method

Table 1 provides the results of the batch least-squares technique. The first column gives the number of measurement points, equidistant in time over an orbital revolution. Therefore, the intervals between the successive data points range from 72 deg (i.e., 4.8 h) in the first row to 0.36 deg (i.e., 8.6 s) in the final row. We did not perform any preprocessing of the data, for instance, by averaging the individual measurements, which arrive every 0.66 s, before applying the least-squares method.

The second column gives the angular deviation of the resulting least-squares attitude relative to the reference attitude used by ESOC (i.e., $\alpha = 83.265$ deg, $\delta = 86.492$ deg, see [9] p. 66).

The third column provides the estimate of the coefficient c_0, which represents the average of the function $y(\nu)$ over the orbit and is a useful parameter for the bias analyses. The next column provides the mounting parameter $b = c_0/\cos\rho_c$, which follows directly from the c_0 estimate. The final column gives the reconstructed bias mounting angle $\Delta\mu$ that reconciles [in accordance with Eq. (62)] the differences between the observed values of the parameters c_0 and b with their assumed baseline values.

The results of the second column of Table 1 show that, initially at least, the results of the least-squares estimation technique approach the ESOC reference attitude for an increasing number of measurements. However, in the lower part of Table 1 when over 100 data points are used, there is apparently no further convergence. The lack of further convergence towards the ESOC attitude may be surprising at first sight. However, it must be kept in mind that the actual attitude is unknown and that the ESOC attitude, which is used for comparisons sake, differs also from the real attitude. The outlier results for the 600 and 1000 points in Table 1 indicate the presence of

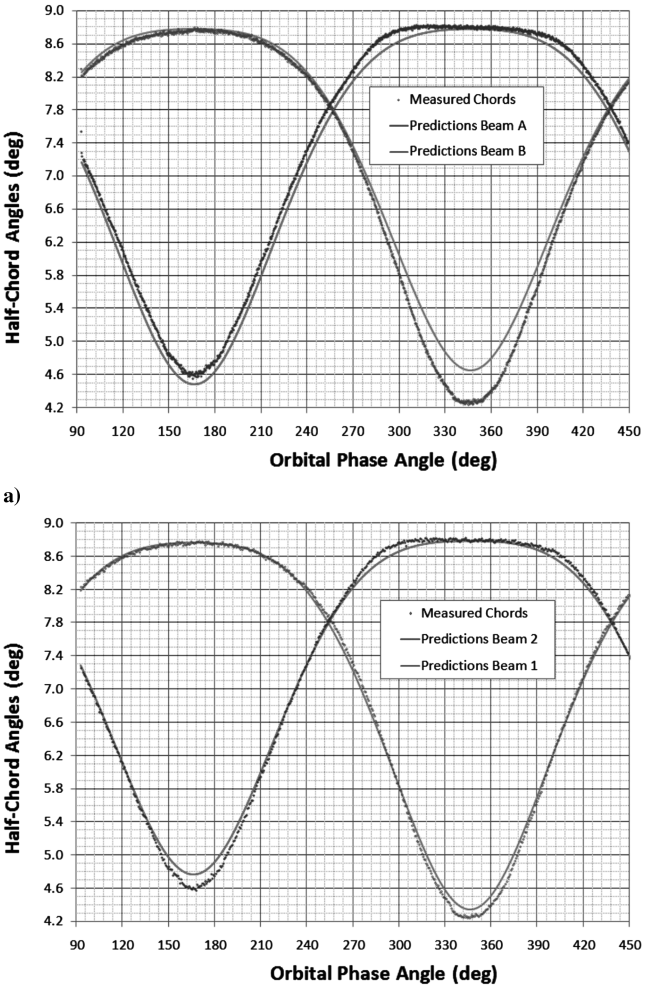

Fig. 7 Measured and predicted half-chord angles before and after correction.

unmodeled bias effects like the Earth's infrared radius and the spin-axis wobbling motion.

In any case, the results for the c_0 estimate and the associated reconstructed b and $\Delta\mu$ parameters in Table 1 remain very stable after about 30 data points.

The result of $\Delta\mu$ in Table 1 points to the presence of a bias in the sensor mounting angle. The value of this bias will be taken as $\Delta\mu = 0.18$ deg so that we have $\mu \approx 90.13$ deg instead of its nominal value of $\mu \approx 89.95$ deg. The value of 0.18 deg is preferred over the result from Table 1 (i.e., ≈ 0.20 deg) because it produces more uniform residuals and a better symmetry between the residuals near the extremes of the chords. In fact, the reconstructed $\Delta\mu$ bias is more likely due to a dynamical tilt in the spin axis, caused by asymmetrical propellant loading in the tanks, rather than an actual offset in the sensor mounting angle. Furthermore, it should be noted that the selected $\Delta\mu$ bias will likely also contains significant contributions from other unmodeled effects, in particular those induced by variations in the Earth's infrared radius, which is expected to be the predominant bias in the present application.

C. Reconstruction of Biases from Residuals

Figures 7 and 8 show the residuals in the half-chord measurements and in the function $y(\nu)$, respectively. Figures 7a and 8a are based on the a priori sensor mounting angles, whereas Figs. 7b and 8b use mounting angles that have been corrected for the reconstructed $\Delta\mu$ bias as discussed previously.

Figures 9a and 9b provide close-ups of the observed residuals in Figs. 7b and 8b. Variations of up to almost 0.2 deg in the half-chord-length angles are visible now. These residuals are believed to be largely due to local variations in the Earth's infrared radius. It is known [8] that the Earth radiance may vary strongly as a function of the Earth-aspect angle. Also, systematic offsets in the sensor mounting angles and, more likely, dynamical imbalance of the spin axis, contribute to these residuals. The higher frequency wobbling of the spin axis mentioned previously can also be observed in the residuals (see also [9], pp. 60–61). Unfortunately, the residuals yield little quantitative information on the relative contributions of the various biases.

The ad hoc approaches for estimating the attitude and for reconstructing some of the biases that are proposed at various stages in this paper produce useful results in general. For instance, the determination of the attitude declination from the extremes in the chords in Eq. (36) is only 0.08 deg away from the ESOC attitude result. The determination of the attitude right ascension from the two equal-chord locations produces two results that are essentially equal and about 0.15 deg away from the ESOC reference attitude. Because the different attitude solutions are within 0.1 deg of each other, it is likely that the actual (unknown) attitude error may be of a similar small order of magnitude.

The reconstruction of the uniform Earth-radius bias from the two equal-chord measurements in the orbit [Eq. (64)] with average value $\Delta\kappa_c = 0.042$ produces $\Delta\rho_c = 0.038$ deg. This corresponds to an offset in the Earth horizon of about 24 km. The value of $\Delta\kappa$ can be seen to be consistent with the residuals in the neighborhood of the two equal-chord points in Fig. 9a.

Finally, the reconstruction of the parameter b from the measured extremes in the function $y(\nu)$ by means of Eq. (35) produces

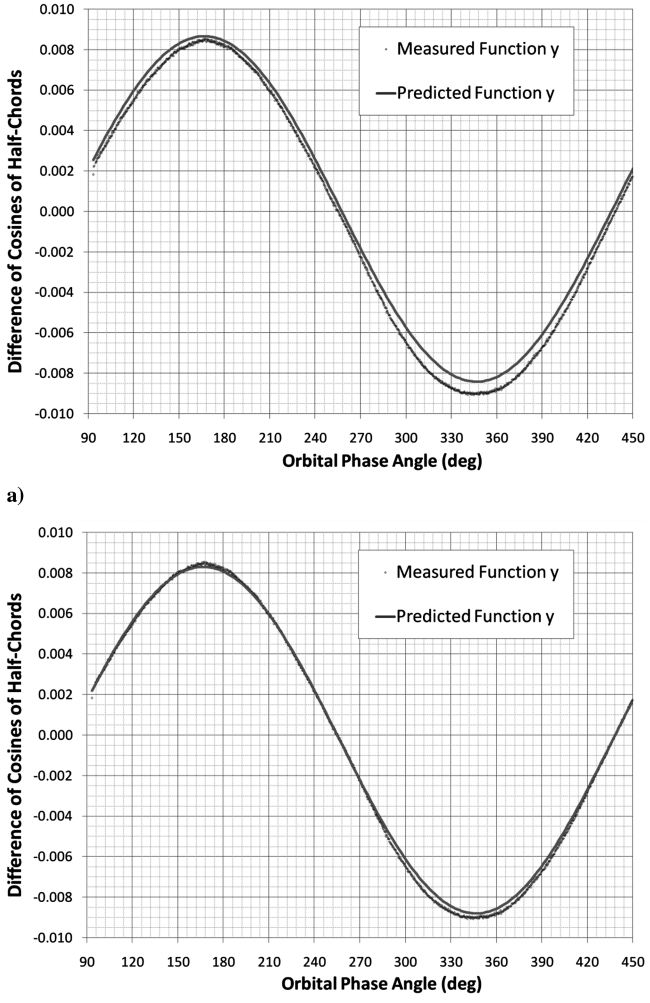

Fig. 8 Measured and predicted function $y(\nu)$ before and after correction.

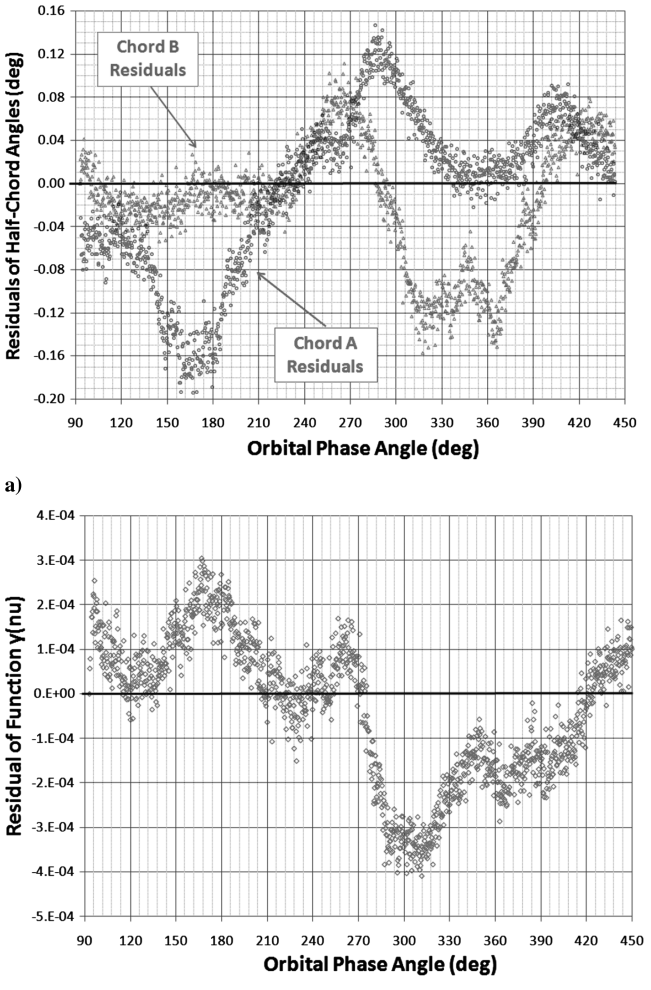

Fig. 9 Observed residuals in half-chord angles and in function $y(\nu)$.

$b = -2.6 \times 10^{-4}$, which is different from the more credible averaged result $b = -3.7 \times 10^{-4}$ found in Table 1. It is reassuring that the discrepancy of 1.1×10^{-4} may be attributed to the asymmetry in the residuals of the function $y(\nu)$ near the chord extremes at $\nu \approx 165$ and 345 deg in Fig. 9b.

IX. Conclusions

The paper presents an outline of the principles and the implementation aspects of a few straightforward techniques for spin-axis attitude determination based on the orbital variations in the half-chord-angle measurements produced by the Earth-sensor pencil beams. The spin-axis attitude can be established directly from the observed magnitudes and phases of the extremes in the chord-angle variations over the orbit. Furthermore, an effective least-squares approach is presented that employs a number of equidistant chord-angle measurements over the orbit. These methods do not require any a priori attitude knowledge or any additional measurements from a different sensor. We also present results for the sensitivity of the attitude solution to the most relevant biases affecting the chord-angle measurements and a few approaches for the reconstruction of these biases. The application of the techniques has been illustrated by using actual sensor data from the geostationary MSG-2 weather satellite. The results demonstrate that the proposed methods offer straightforward, effective, and attractive alternatives to the traditional attitude estimation methods.

Acknowledgment

The authors are grateful to A. Schuetz and Xavier Marc of ESA/European Space Operations Centre for providing the MSG-2 in-orbit data and for additional background information.

References

[1] Wertz, J. R. (ed.), *Spacecraft Attitude Determination and Control*, Springer–Verlag, New York, 1978, Chaps. 10–14.

[2] Shuster, M. D., "Efficient Algorithms for Spin-Axis Attitude Estimation," *The Journal of the Astronautical Sciences*, Vol. 31, No. 2, April–June 1983, pp. 237–249.

[3] Tanygin, S., and Shuster, M. D., "Spin-Axis Attitude Estimation," *The Journal of the Astronautical Sciences*, Vol. 55, No. 1, 2007, pp. 107–139.

[4] van der Ha, J. C., "Equal-Chord Attitude Determination Method for Spinning Spacecraft," *Journal of Guidance, Control, and Dynamics*, Vol. 28, No. 5, Sept.–Oct. 2005, pp. 997–1005. doi:10.2514/1.10660

[5] van der Ha, J. C., "Spin Axis Attitude Determination Accuracy Model in the Presence of Biases," *Journal of Guidance, Control, and Dynamics*, Vol. 29, No. 4, July–Aug. 2006, pp. 799–809. doi:10.2514/1.17745

[6] Crassidis, J. L., and Junkins, J. L., *Optimal Estimation of Dynamic Systems*, CRC Press, Boca Raton, FL, 2004, Sec. 1.2.

[7] van der Ha, J. C., Rogers, G., Dellinger, W., and Stratton, J., "CONTOUR Phasing Orbits: Attitude Determination & Control Concepts & Flight Results," *Advances in the Astronautical Sciences*, Vol. 114, Part II, 2003, pp. 767–782.

[8] De Juana Gamo, J. M., Mugellesi–Dow, R., Schuetz, A., Hocken, D., Schwarz, L., and Soerensen, A., "MSG-2 Mission and Flight Dynamics Operations," *25th International Symposium on Space Technology and Science*, International Symposium on Space Technology and Science, Paper 2006-d-28, Kanazawa, Japan, June 2006.

[9] Attitude Determination, MSG-2 LEOP Flight Dynamics Report MSG2-FDOS-AD-FDR-0001-OPERATIONS-GFM, ESA/European Space Operations Centre, Darmstadt, Germany, 14 Feb. 2006.

[10] van der Ha, J. C., and Lappas, V. J., "Long-Term Attitude Drift of Spinning Spacecraft Under Solar Radiation Torques," *Journal of Guidance, Control, and Dynamics*, Vol. 30, No. 5, Sept.–Oct. 2007, pp. 1470–1479. doi:10.2514/1.28506